Permanent-Magnets Linear Actuators Applicability in Automobile Active Suspensions

Ismenio Martins, *Member, IEEE*, Jorge Esteves, *Senior Member, IEEE*, Gil D. Marques, *Member, IEEE*, and Fernando Pina da Silva

***Abstract*—Significant improvements in automobile suspension performance are achieved by active systems. However, current active suspension systems are too expensive and complex. Developments occurring in power electronics, permanent magnet materials, and microelectronic systems justifies analysis of the possibility of implementing electromagnetic actuators in order to improve the performance of automobile suspension systems without excessively increasing complexity and cost. In this paper, the layouts of hydraulic and electromagnetic active suspensions are compared. The actuator requirements are calculated, and some experimental results proving that electromagnetic suspension could become a reality in the future are shown.**

***Index Terms*—Active suspension, automobile suspension, linear actuator, permanent magnet.**

I. Introduction

THE use of electromagnetic linear actuators in automobile suspensions has already been proposed by other authors. The reliability of electrical drives and unconstrained integration with electronic control systems are very important factors that justify the generalized use of electromagnetic actuators in automobile suspensions.

Earlier attempts at using electromagnets in electromagnetic automobile suspension were made by Tall in 1961 and Lyman in 1966 [1] and [2]. Lately, several authors have proposed other kinds of electromagnetic systems for automobile suspensions based on a rotational actuator [3]–[8]. However, the use of rotational actuators requires a gearbox to convert the rotational into linear movement and to increase the force value.

Linear actuators do not require any kind of gearbox. The first automobile suspension systems using linear actuators were proposed in [9]–[16].

Other works describing the advantages of electrical suspensions and linear permanent magnets actuators have also been published [17]–[19].

The main objective of ground vehicle suspension systems is to isolate the vehicle body from road irregularities in order to maximize passenger ride comfort and to produce continuous road-wheel contact, improving the vehicle handling quality [20].

Manuscript received November 13, 2001; revised June 28, 2004. This work was supported by the project PRAXIS/P/EEEI-14270/1998, named "Electromagnetic Vehicle Suspensions" funded by the PRAXIS Program and Portuguese FCT. The review of this paper was coordinated by Dr. M. Abul Masrur.

I. Martins is with the Escola Superior de Tecnologia, University of Algarve, 8000 Faro, Portugal (e-mail: imartins@ualg.pt).

J. Esteves, G. D. Marques, and F. P. da Silva are with the Instituto Superior Técnico-Technical University of Lisbon, 1049-001 Lisbon, Portugal (e-mail: jesteves@erse.pt; gil.marques@ist.utl.pt; fpsilva@dem.ist.utl.pt).

Digital Object Identifier 10.1109/TVT.2005.861167

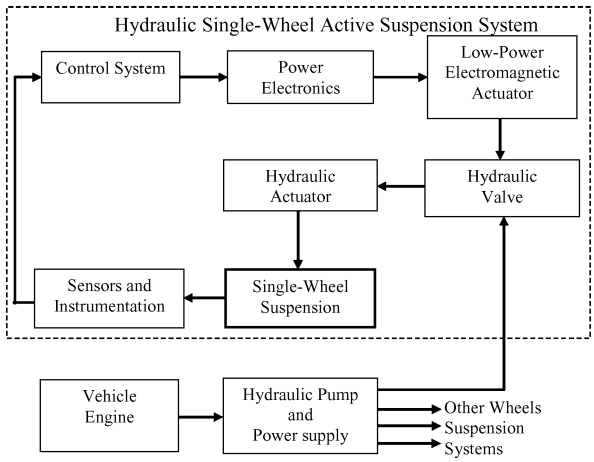

Fig. 1. Block diagram of a hydraulic single-wheel active suspension.

Currently, three types of vehicle suspensions are used: passive, semi-active and active. All systems implemented in automobiles today are based on hydraulic or pneumatic operation. However, it is found that these solutions do not satisfactorily solve the vehicle oscillation problem, or they are very expensive and increase the vehicle's energy consumption [14] and [18].

Significant improvement of suspension performance is achieved by active systems. However, these are only used in a small number of automobile models because they are expensive and complex.

In Fig. 1, a block diagram of a single-wheel hydraulic automobile active suspension is presented. The vehicle engine drives a hydraulic pump to power the suspension based on hydraulic actuators that create oscillation-damping forces between the vehicle body and the wheel assembly. A hydraulic valve is driven by a low-power electromagnetic actuator in order to handle the actuator forces. The control system, together with a power electronics converter, drives the low-power electromagnetic actuator.

In the last ten years, developments in power electronics, permanent magnet materials, and microelectronic systems have brought significant improvements in the electrical drive domain. Increases in dynamic and steady-state performances, reductions in volume and weight, unconstrained integration with electronic control systems, reliability, and cost reduction are important factors that justify the generalized use of electrical drives.

This evolution justifies an analysis of implementing suspension systems using electromagnetic actuators in order to improve the performance without increasing energy consumption or costs.

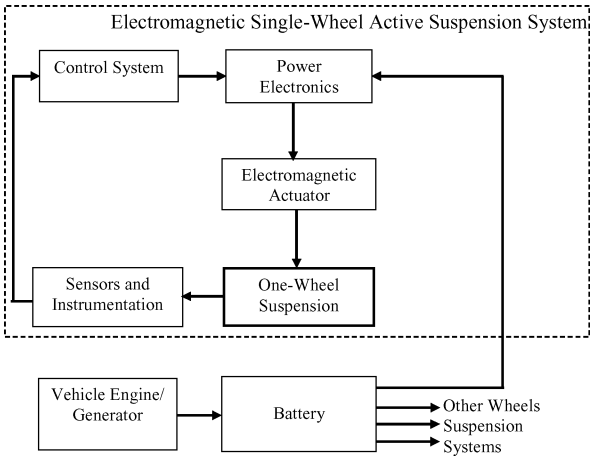

Fig. 2. Block diagram of an electromagnetic single-wheel automobile active suspension.

In Fig. 2, a block diagram of an automobile suspension using an electromagnetic linear actuator is shown. An electrical generator feeding a battery now replaces the complex and expensive hydraulic power supply. The hydraulic valve and actuator have been removed from the system. An electromagnetic actuator driven by the control system through a power electronics converter is the main component of the wheel suspension system.

The actuator and power electronics must be larger in this case. However, the system is simpler since it has fewer devices and mechanical parts. Because it has no hydraulic devices, this is an oil-free system.

This paper shows that it is now possible to build an electromagnetic actuator producing the required forces and with suitable power and dimensions for this application.

II. Actuator Requirements

A. Active Suspension Models

1) Hydraulic Suspension: Fig. 3 presents a model for vehicles with independent suspensions, where m_s represents a quarter of the "sprung" mass of a vehicle, m_u the "unsprung" mass of one wheel with the suspension and brake equipment, k_s the spring stiffness, k_t the tire stiffness, and b_s the damper coefficient. The variable F_f represents the friction force [21].

The dynamic behavior of a single-wheel suspension system may be expressed by the following differential equations:

$$m_s \ddot{z}_s = -k_s(z_s - z_u) - b_s(\dot{z}_s - \dot{z}_u) - F_f + F_A \tag{1}$$

$$m_u \ddot{z}_u = k_s(z_s - z_u) + b_s(\dot{z}_s - \dot{z}_u) - k_t(z_u - z_r) + F_f - F_A. \tag{2}$$

The force of the hydraulic actuator is represented by F_A. The actuator force law (3) is defined as in [21] and [22] and is given by

$$F_A = -C\dot{z}_s \tag{3}$$

where C is a constant coefficient.

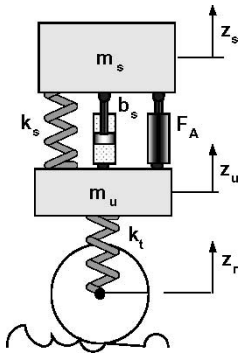

Fig. 3. Model of a hydraulic single-wheel active suspension.

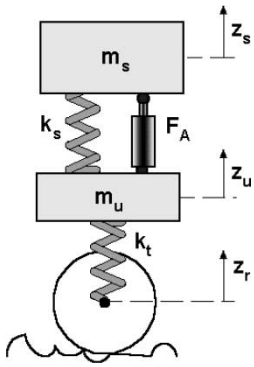

Fig. 4. Model of an electromagnetic single-wheel active suspension.

2) Electromagnetic Suspension: The electromagnetic actuator replaces the damper and the hydraulic actuator, forming with the spring an oil-free suspension. Fig. 4 presents a model of an electromagnetic suspension [16].

The friction force of an electromagnetic actuator can be neglected. So, the dynamical equations of the suspension system become

$$m_s \ddot{z}_s = -k_s(z_s - z_u) + F_A \tag{4}$$

$$m_u \ddot{z}_u = k_s(z_s - z_u) - k_t(z_u - z_r) - F_A \tag{5}$$

and the electromagnetic actuator force law, to obtain the same dynamics as the hydraulic suspension, results

$$F_A = -b_s(\dot{z}_s - \dot{z}_u) - C\dot{z}_s. \tag{6}$$

3) Control System: The control system must ensure the calculation of an actuator reference force F_{Aref}, in conformity with expression (3) in the case of a hydraulic suspension, or with (6) in the case of an electromagnetic active suspension. The actuator, power electronics converter, mechanical components, and instrumentation feedback are also parts of the closed-loop automatic control electromagnetic suspension system. The suspension dynamics is governed mostly by the actuator force and by the suspension mechanics, in accordance with (4) and (5).

In Fig. 5, the electromagnetic active suspension control system diagram is shown. The force reference is obtained from the sprung and unsprung speeds, related to a zero vertical speed point fixed on the sky (skyhook speeds) [21]. A coefficient

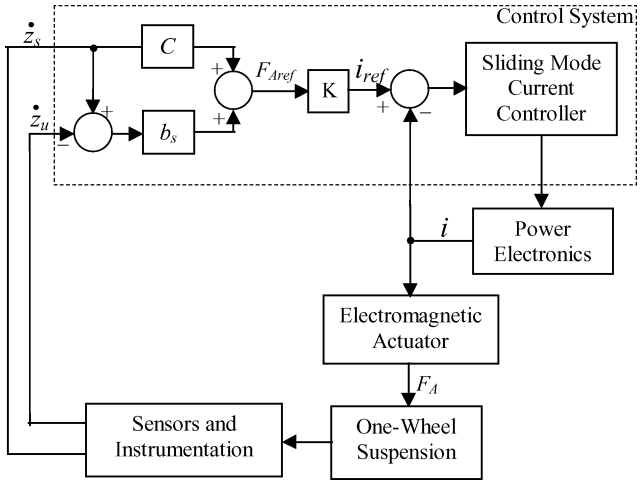

Fig. 5. Electromagnetic active suspension control system.

$K = 1/K\Phi$, related to the actuator construction parameters and to the magnetic field, enables the reference current to be calculated, correspondingly to the required force. The current value is controlled by a sliding mode controller [23].

B. Suspension Forces

1) Critical Working Points: Resonance frequencies are the most critical working points not only from the standpoint of comfort and safety but also for the design of the actuator power and force values. These frequencies, given by expressions (7) and (8), are the natural frequency values of the two suspension subsystems: the "suspension spring stiffness/sprung mass" and the "tire stiffness/unsprung mass" [20].

$$f_{S0} = \frac{1}{2\pi}\sqrt{\frac{k_s}{m_s}} \tag{7}$$

$$f_{U0} = \frac{1}{2\pi}\sqrt{\frac{k_t}{m_u}}. \tag{8}$$

2) Actuator Stroke, Velocity, and Force Values: The parameters needed for the actuator design were obtained by systematic use of numerical simulations. These include stroke and velocity values, peak and rms force and power values.

The numerical simulation of (4) and (5), using the control law (6), was conducted with parameters from [21] and [22]. These parameters are presented in Table I.

In the first stage, the actuator forces were investigated in simulation, using a 1.2-Hz frequency and a 1-in amplitude sinusoidal wave as road input disturbance. This amplitude is normally used in published works on this subject [22] and others. The frequency chosen is approximately the sprung-mass resonance frequency, which is also normally used to verify suspension operation.

The actuator parameters for the analyzed case are presented in Table II. Simulation results of the instantaneous force are presented in Fig. 6.

Although in most situations the suspension input-disturbance z_r is smooth, suspensions must operate in a large spectrum of input disturbance frequency values due to road irregularities, which creates a set of frequencies of distinct amplitudes. The most significant of these frequencies are the resonance frequencies of the sprung and unsprung masses.

The ISO 2631 standard gives the acceptable time period exposure of a car passenger to a set of vertical acceleration levels. These vibration levels are set in terms of rms acceleration values that produce equal "fatigue-decreased proficiency." In most situations, exceeding the specified exposure causes noticeable fatigue and may be a cause of a large number of automobile crashes. In the above standard, the rms acceleration upper bound is taken to be twice the "fatigue-decreased proficiency" levels.

TABLE I
SUSPENSION SIMULATION PARAMETERS

Symbol	Quantity	Value
m_s	Sprung mass	290 kg
m_u	Unsprung mass	59 kg
k_s	Spring stiffness	16 812 N/m
k_t	Tire stiffness	190 000 N/m
b_s	Damper coefficient	1000 N/m/s
C	Active force coefficient	3000 N/m/s

TABLE II
SIMULATION RESULTS FOR A 1.2-Hz FREQUENCY AND A 1-IN AMPLITUDE INPUT DISTURBANCE

Quantity	Value
Max. stroke	50 mm
Max. velocity	0.28 m/s
Peak force	450 N
RMS force	295 N
Peak power	65 W
RMS power	37 W

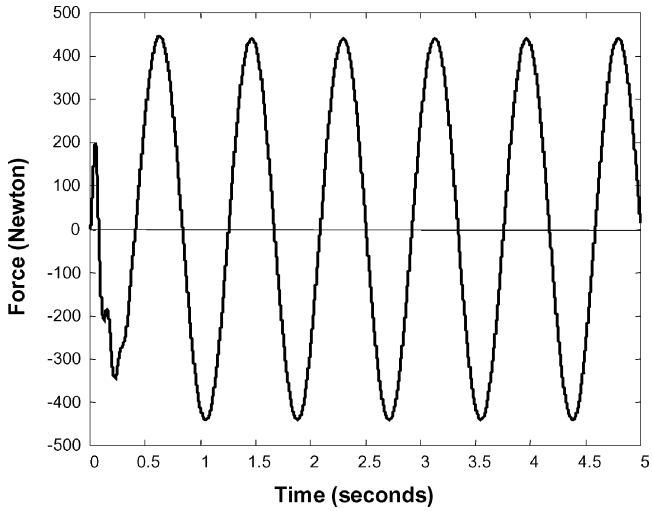

Fig. 6. Active suspension actuator instantaneous force, using a sinusoidal road perturbation of 1.2-Hz frequency and 2.54-cm amplitude.

TABLE III
SIMULATION RESULTS FOR THE REDUCED COMFORT BOUNDARY

Quantity	1.2 Hz / 1.5 cm 9 Hz/ 0.05 cm	1.2 Hz / 3.5 cm 9 Hz/ 0.15 cm	1.2 Hz / 8.5 cm 9 Hz/ 0.25 cm
Reduced comfort time boundary	4 h	1 h	1 min
Max. stroke	32 mm	80 mm	160 mm
Peak force	350 N	900 N	2000 N
RMS force	186 N	451 N	1041 N
RMS power	21 W	139 W	615 W

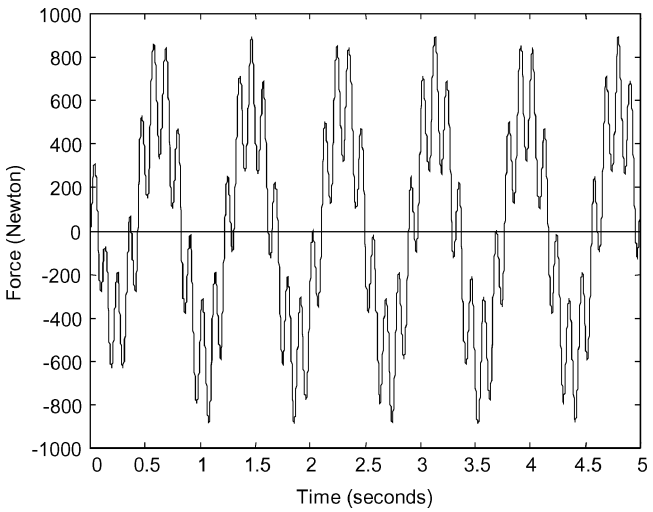

Fig. 7. Active suspension actuator instantaneous force, using a set of two sinusoidal road perturbation waves of 1.2 Hz, 3.5-cm amplitude and 9-Hz, 0.15-cm amplitude.

The "reduced comfort boundary" is assumed to be about one-third of the standard levels [24].

Automobile drivers automatically avoid the set of "reduced comfort boundary" frequencies values, simply because they feel uncomfortable, by decreasing or increasing the vehicle's speed. Consequently, the sprung-mass acceleration levels are normally below the levels defined as the "reduced comfort boundary." These considerations were used to define the actuator steady-state power.

For calculation of the actuator steady-state operation upper limits, a numerical simulation of the suspension model was conducted. As model disturbance, a combined signal was used composed of the sum of two sinusoidal waves with different amplitudes and frequencies. These are, respectively, the sprung and unsprung mass resonance frequencies. The numerical simulation results, conducted for three amplitude sets, are presented in Table III. For each frequency-amplitude set, the "reduced comfort boundary" time was found, as shown in Table III.

In Fig. 7, the instantaneous force simulation result is presented.

TABLE IV
ACTUATOR DESIGN PARAMETERS

Quantity	Value
Stroke	160 mm
Steady-state force	1000 N
Peak velocity	1.2 m/s
RMS power	615 W
Max. diameter	150 mm
Max. length	600 mm

III. ACTUATOR DESIGN CONSIDERATIONS

From Tables II and III, and for the suspension parameters presented in Table I, one can define the actuator operation limits for an electromagnetic active suspension. The actuator should be able to produce an rms force value of 1050 N in the steady state. Its stroke should be 160 mm, and the peak velocity is about 1.2 m/s.

A. Maximum Dimensions and Shape

The actuator must fit in a reasonable space, near the wheel. The available room for the actuator depends on the car design. So, it cannot be defined exactly, except for a specific model.

At present, a cylindrical shape seems to be the most suitable because cars are designed to use hydraulic or pneumatic actuators, and these have a cylindrical shape. Moreover, this shape allows the use of helical sprigs around the actuator, and it can be an advantage for the suspension design.

The design parameters for an experimental electromagnetic actuator are presented in Table IV.

B. Actuator Layout

A cylindrical permanent-magnet linear actuator can be built in two possible configurations: moving magnets or moving coils [19]. However, in an automobile suspension, to define precisely a non-moving part is not possible. In fact, both parts of the actuator are in movement, because one is connected to the sprung mass, and the other to the unsprung mass. However, a moving part can be taken to be the part connected to the unsprung mass.

It is better to put the coils on the sprung mass side because this is the vehicle body side. On the other hand, it is advantageous for suspension performance to have less actuator weight on the unsprung mass side. Developments in high-energy NdFeB magnets allow the construction of reasonable magnetic excitation arrangements [19].

The moving-magnet cylindrical linear actuator can be constructed using radial or axially magnetized permanent magnets.

In the first case, as shown in Fig. 8(a), the magnetic poles are obtained by assembling radial magnetized NdFeB rings on a magnetic-steel rod. In the second case, in Fig. 8(b), two opposite-field NdFeB axially magnetized cylinders are assembled sandwiching a magnetic-steel cylinder. The magnetic field crosses the cylinder tops and then the cylindrical surface.

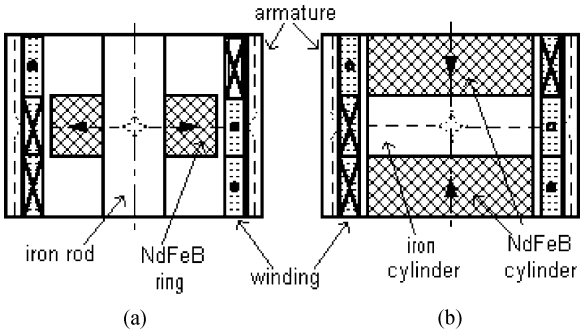

Fig. 8. Actuator configurations. (a) Radial magnetization. (b) Axial magnetization.

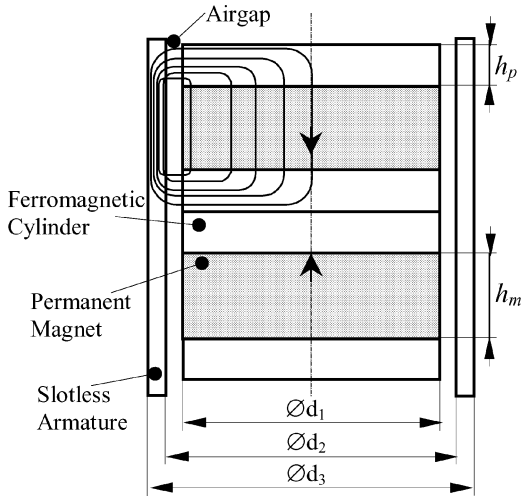

Fig. 9. Linear actuator magnetic circuit configuration.

In both configurations, copper windings are assembled inside a longitudinally laminated silicon-magnetic-steel slotless armature. The air gap is thus the distance between the poles and the armature, with the copper windings and their electrical insulation almost filling it.

Radially magnetized NdFeB magnets are very expensive compared to axially magnetized magnets. Both configurations were analyzed, using a finite elements analysis (FEA) program.

C. Actuator Design Analysis

A prototype of a linear permanent magnet cylindrical actuator, using an axial magnet configuration, was designed. The design analysis of this actuator was made using the magnetic circuit configuration shown in Fig. 9. All calculations were made neglecting the magnetic flux leakage. Subsequently, all calculations were confirmed using an FEA program and experimental verification.

The magnetic flux through the permanent magnet top is

$$\Phi = B_m S_m = \frac{B_m \pi \cdot d_1^2}{4}. \tag{9}$$

The magnetic flux density on the ferromagnetic cylinder wall is

$$B_1 = \frac{\Phi}{S_p} = \frac{B_m \pi \cdot d_1^2}{4\pi \cdot h_p d_1} = \frac{B_m d_1}{4h_p} \tag{10}$$

where B_m is the permanent magnet working magnetic flux density medium value.

Having chosen the adequate dimensions for it, one can consider equal medium magnetic flux densities on the ferromagnetic cylinder wall, on the top of the ferromagnetic cylinder, and on the top of the permanent magnet. Therefore

$$B_1 = B_m. \tag{11}$$

From (10) and (11)

$$h_p = \frac{d_1}{4}. \tag{12}$$

Multiple finite-element simulations show that for an NdFeB permanent magnet slotless cylindrical linear actuator, the maximum magnetic energy density is achieved when the air gap volume under the poles is approximately equal to the permanent magnet volume associated to this poles. For the analyzed layout

$$2V_p \approx V_m \tag{13}$$

where V_m is the permanent magnet volume, and V_g is the associated air gap volume.

So, from (13)

$$d_2 = d_1 \sqrt{\frac{h_m}{2h_p} + 1}. \tag{14}$$

In the case of an $h_m = 2h_p$ configuration

$$d_2 = d_1 \sqrt{2}. \tag{15}$$

Taking a magnetic flux value through the armature equal to the magnetic flux value through the ferromagnetic cylinder wall

$$\pi B_m d_1 h_p = \pi B_a d_2 l_a \tag{16}$$

where l_a is the length of the armature wall, and B_a is the armature magnetic flux density.

From (12) and (16)

$$l_a = \frac{B_m d_1^2}{4B_a d_2}. \tag{17}$$

The actuator outside diameter is

$$d_3 = d_2 + 2l_a. \tag{18}$$

From (15), (17), and (18)

$$\begin{cases} d_3 = d_2 + 2l_a \\ d_2 = d_1\sqrt{2} \\ l_a = \frac{B_m d_1^2}{4B_a d_2} \end{cases}. \tag{19}$$

From a given outside actuator diameter d_3, solving (19) was calculated the permanent magnet diameter d_1. The permanent magnet high was calculated from (12).

$$d_1 = \frac{d_3}{\sqrt{2}\left(1 + \frac{B_m}{4B_a}\right)}. \tag{20}$$

The actuator Lorenz force produced by a pair of windings and a permanent magnet

$$F_{2W} = 2 \cdot i\vec{L}_{\mathrm{cu}} \times \vec{B}_g \tag{21}$$

TABLE V
FINITE ELEMENTS ACTUATOR ANALYSIS

Quantity	Radial magnetization	Axial magnetization
Actuator diameter	100 mm	100 mm
Air gap length	11 mm	13 mm
Average flux density near the pole	0.47 T	0.68 T
Average flux density near the armature	0.29 T	0.41 T
One-pole flux	3.04 mWb	4.15 mWb
Non-moving part weight	0.95 kg/coil	0.85 kg/coil
Moving part weight	0.9 kg/pole	1.25 kg/pole
One-coil current	1025 At	1226 At
Force produced	88 N/pole	148 N/pole

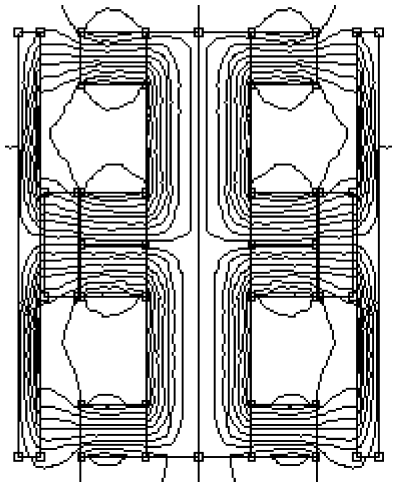

Fig. 10. Flux plot of an actuator pair of poles, using radially magnetized NdFeB permanent magnets.

where $L_{\rm cu}$ is the total conductor length of one winding under the magnetic field, B_g the air gap medium magnetic flux density, and i the windings current, calculated from an allowed current density value, taking into account the actuator cooling system.

Table V presents the parameters used in the calculations and several values obtained from the FEA results.

The actuator final dimensions were calculated from

$$\frac{n_W}{2} \geq \frac{F_A}{F_{2W}} \tag{22}$$

where F_A is the actuator steady state final force, and n_W is the total number of windings under magnetic field.

The coefficient $K\Phi$ was calculated from

$$K\Phi = L_{\rm cu} n_W B_g. \tag{23}$$

Since the actuator is cylindrical, it is axisymmetric and seems that the analysis could be conducted on a two-dimensional plane. However, it was chosen to use tri-dimensional FEA calculations, because the magnetic flux density value varies significantly along the actuator radius. The flux plots obtained from this analysis are presented in Figs. 10 and 11, related to a pair of poles and one winding, for a 100-mm outside-diameter actuator.

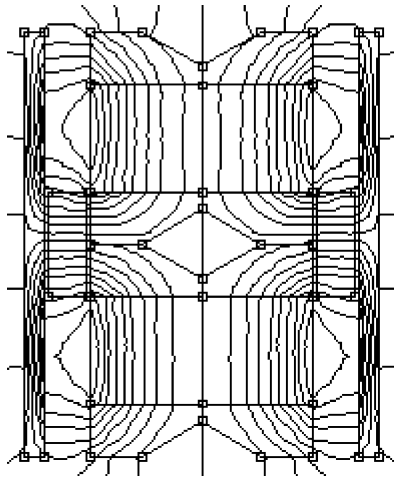

Fig. 11. Flux plot of an actuator pair of poles, using axially magnetized NdFeB permanent magnets.

TABLE VI
EXPERIMENTAL ACTUATOR PARAMETERS

Quantity	Value
Diameter	110 mm
Length	600 mm
Stroke	180 mm
Non-moving part weight	19 kg
Moving part weight	9 kg
Number of poles	7
Number of coils	20
Number of phases	2

IV. PROTOTYPE DESCRIPTION

Based on the above analysis and calculations, a linear actuator was built using axially magnetized NdFeB cylindrical permanent magnets. The experimental actuator parameters are presented in Table VI.

An actuator with these dimensions can fit in the available space near the wheel. However, these values are high, and they are larger than an equivalent hydraulic actuator. A further development in the actuator cooling system could significantly reduce the dimension and weight values presented.

A photograph of the actuator prototype is presented in Fig. 12. Here, the actuator is mounted in a steel structure to measure the produced forces. Fig. 13 shows the laboratory workbench constructed for the evaluation of the actuator as an electromagnetic suspension.

A. Power Electronics Converter

A converter composed of two IGBT full bridges is used to control the current values in the actuator phases. The converter

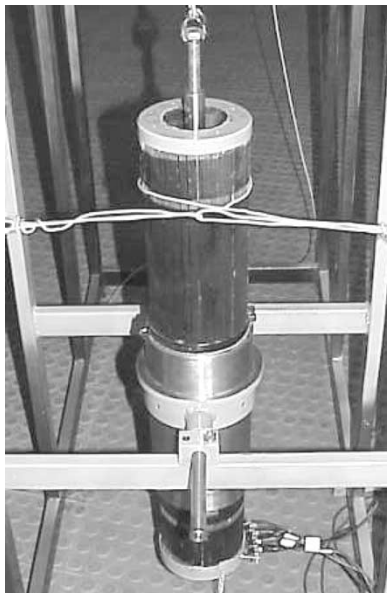

Fig. 12. Actuator prototype.

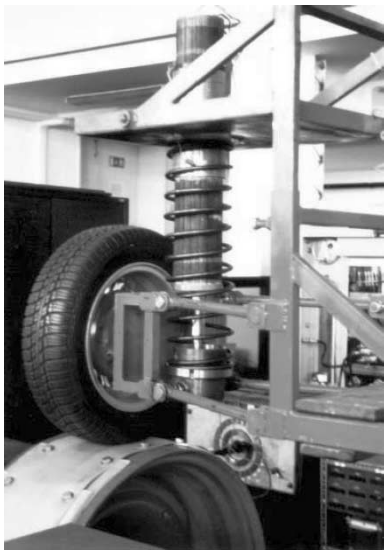

Fig. 13. Actuator prototype and partial view of the workbench.

layout is shown in Fig. 14. The inductances represented in the figure are the actuator phase inductances added to the external inductances in order to limit the current gradient. In the prototype, $L_1 = L_2 = 5$ mH.

The semiconductor switches work in accordance with a sliding mode control law [23]. So, the voltage output value of each phase is given by

$$U(t) = \begin{cases} +U, & \text{if } \delta i > \Delta i \\ -U, & \text{if } \delta i < \Delta i \end{cases}. \tag{24}$$

The commutation frequency maximum of each IGBT can be calculated by

$$f_{\max} = \frac{U_{\max}}{4\Delta i L}. \tag{25}$$

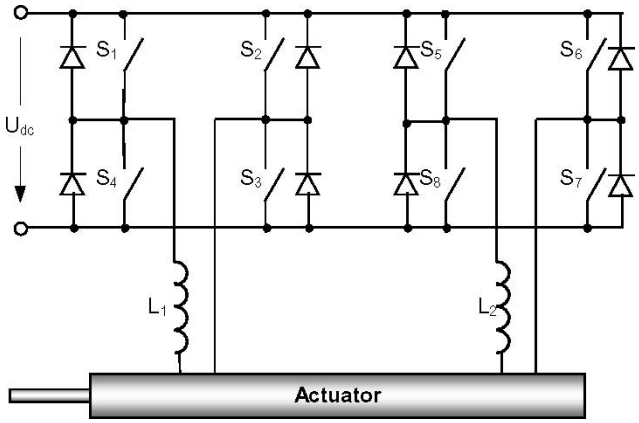

Fig. 14. Power electronics converter layout.

For a set of 50-V supply voltage and $\Delta I = 500$ mA, a maximum of 5-kHz commutation frequency was found.

B. Phase Current Control

The finite elements analysis shows that the radial magnetic induction in the windings along the actuator has a sinusoidal variation. So, the currents should also have a sinusoidal variation, in order to ensure an optimal linear relation between the current and the force. As it is a two-phase winding system, the current of one phase must be shifted by an arc angle of $\pi/2$ relative to the other phase.

The current should be dependent upon the position of the poles, relative to the windings. An LVDT sensor was used to measure the distance between the sprung and unsprung masses. This distance is calculated from

$$(z_s - z_u) = U_{\mathrm{LVDT}} K_{\mathrm{LVDT}} \tag{26}$$

where U_{LVDT} is the sensor-output voltage value, and K_{LVDT} is a constant coefficient. The equivalent position angle is obtained from

$$\theta = \frac{U_{\mathrm{LVDT}} K_{\mathrm{LVDT}}}{2h}\pi + \frac{\pi}{2} \tag{27}$$

where h is the pole length. A phase current control functional diagram is shown in Fig. 15.

In Fig. 16, the experimental results of the force values produced by the actuator prototype versus the current per phase are shown.

V. Experimental Results

The input disturbance is produced with an appropriate workbench drum surface (Fig. 13). The input obtained is an almost sinusoidal perturbation with a frequency value of 3.28 Hz and amplitude equal to 8 mm. However, as presented in Fig. 17, the obtained disturbance amplitude spectrum also shows some frequency components.

Experimental results of the linear actuator working as a passive suspension system are shown in Figs. 18 and 19. In this simpler system, the actuator is working as an electric generator. Each actuator phase is connected to an external power resistor. No power electronics are connected. In this configuration, with

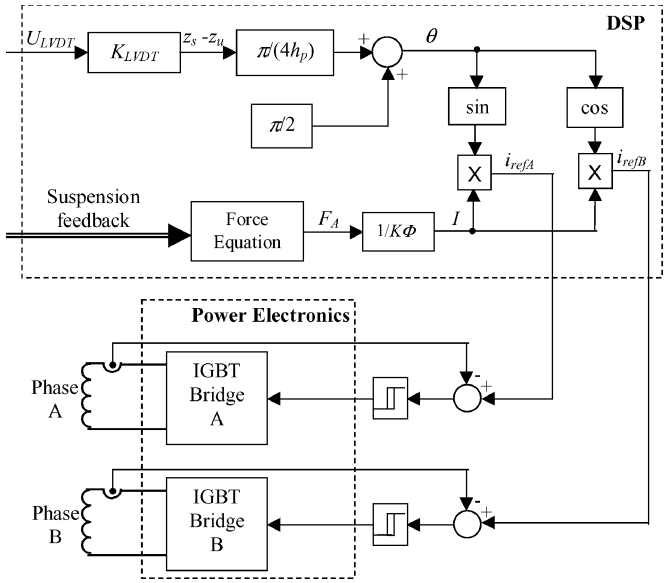

Fig. 15. Phase current control functional diagram.

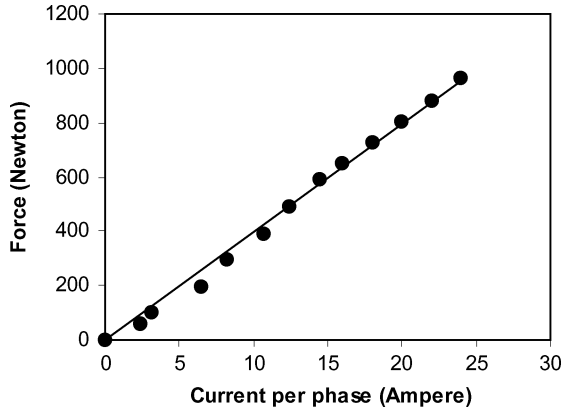

Fig. 16. Force produced by the actuator prototype versus the current per phase.

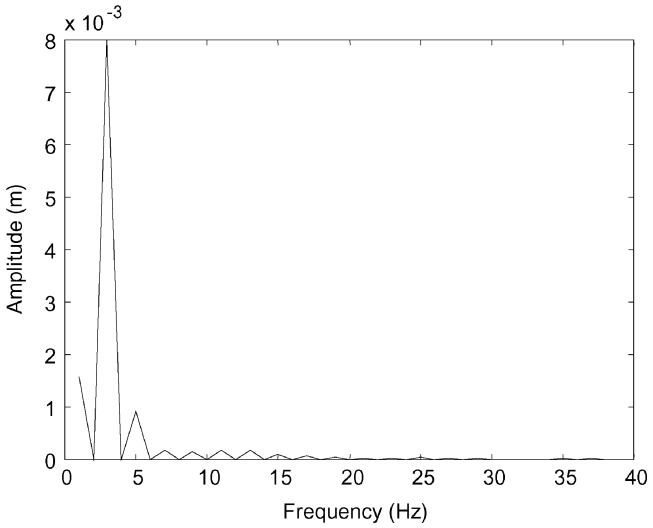

Fig. 17. Disturbance amplitude spectrum obtained from FFT analysis of the workbench irregularities profile.

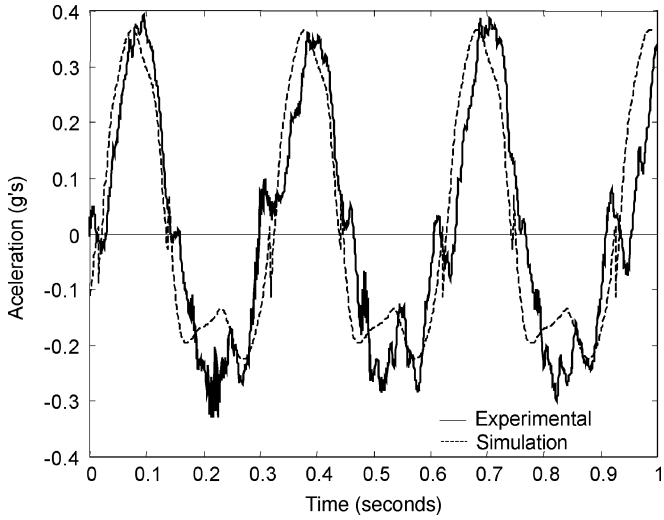

Fig. 18. Sprung mass acceleration.

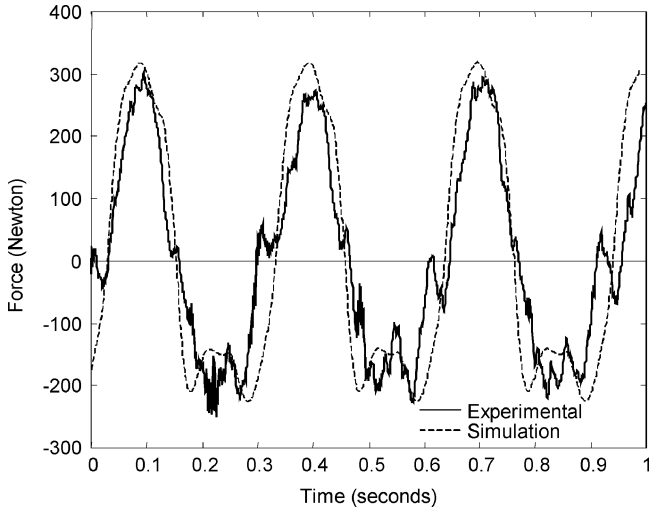

Fig. 19. Force produced by the actuator.

the resistors connected to the armature, the system is equivalent to a 1350-N/m/s damping coefficient.

The sprung mass acceleration presented in Fig. 15 shows that the actuator can operate as a passive suspension, damping the oscillations caused by the ground irregularities. The obtained sprung mass acceleration peak values are in agreement with what is expected for a passive suspension.

Fig. 16 shows the evolution of the force produced by the actuator. In general, the experimental results obtained validate the simulation model used. The experiments also show the capability and applicability of this kind of linear permanent magnet actuator for automotive suspension systems.

VI. Conclusion

The analysis and the experimental results presented here show that it is possible to build an electromagnetic actuator suitable for application in an automobile electromagnetic suspension. It is shown that the force values produced by the actuator are

suitable for the proposed application. The constructed actuator is oil-free and does not need any kind of hydraulic system.

Although the dimensions and the weight are suitable, these values are larger than an equivalent hydraulic actuator. However, further development in the actuator cooling system could significantly reduce the dimension and weight values presented. For instance, the performance of a water-cooled actuator should be investigated.

The utilization of this electrical drive system in the automobile suspensions allows a relatively easy implementation of an active control suspension law. Furthermore, the application of other control laws allowing improvements in the automotive suspension performance becomes possible.

ACKNOWLEDGMENT

Acknowledgments are due to the authors of the finite elements analysis program Finite Element Method Magnetic (FEMM).

REFERENCES

[1] A. P. Yankowski and A. Klausner, "Electromagnetic shock absorber," U.S. Patent 3 941 402, Mar. 2, 1976.
[2] C. Theodore and J. A. Ross, "Suspension dampening for a surface support vehicle by magnetic means," U.S. Patent 3 842 753, Oct. 1974.
[3] W. C. Kruckemeyer, H. C. Buchanan, Jr., and W. V. Fannin, "Rotational actuator for vehicle suspension damper," U.S. Patent 4 644 200, Feb. 17, 1987.
[4] B. V. Murty, "Electric, variable damping vehicle suspension," U.S. Patent 4 815 575, Mar. 28, 1989.
[5] B. V. Murty and R. R. Henry, "Active vehicle suspension with brushless dynamoelectric Actuator," U.S. Patent 5 091 679, Feb. 25, 1992.
[6] R. R. Henry, M. A. Applebee, and B. V. Murty, "Full car semi-active suspension control based on quarter car control," U.S. Patent 5 475 596, Dec. 12, 1995.
[7] D. A. Weeks, D. A. Bresie, J. H. Beno, and A. M. Guenin, "The design of an electromagnetic linear actuator for an active suspension," in *Proc. SAE Steering and Suspension Technology Symp*., Detroit, MI, 1999, pp. 1–11.
[8] J. H. Beno, D. A. Weeks, and W. F. Weldon, "Constant force suspension, near constant force suspension, and associated control algorithms," U.S. Patent 5 999 868, Dec. 7, 1999.
[9] Z. Kurtzman, "Electromagnetic strut assembly," European Patent Application EP 0 343 809 A2, 1989.
[10] K. O. Stuart, "Electromagnetic actuator," U.S. Patent 4 912 343, Mar. 27, 1990.
[11] K. O. Stuart and D. C. Bulgatz, "Electromagnetic Actuator," U.S. Patent 5 187 398, Feb. 16, 1993.
[12] P. Denne, "Motion control systems," International Patent WO 95/16253, Jun. 1995.
[13] J.-J. Charaudeau, D. Laurent, and J.-L. Linda, "Suspension device comprising a spring corrector," U.S. Patent 6 161 844, Dec. 19, 2000.
[14] I. Martins, J. Esteves, and F. P. da Silva, "Energy recovery from an electrical suspension for EV," in *Proc. Electric Veh. Symp., EVS-15*, Brussels, Belgium, 1998.
[15] ——, "Electromagnetic hybrid active-passive vehicle suspension system," in *Proc. IEEE Veh. Tech. Conf. VTC'99*, Houston, TX, vol. 3, 1999, pp. 2273–2277.
[16] I. Martins, J. Esteves, F. P. da Silva, and A. Tomé, "Automobile suspensions using electromagnetic linear actuators," in *Proc. IFAC Conf. Mechatronics*, Darmstadt, Germany, 2001, pp. 203–208.
[17] J. G. Kassakian, H.-C. Wolf, J. M. Miller, and C. J. Hurton, "Automotive electrical systems circa 2005," *IEEE Spectrum*, vol. 33, no. 8, pp. 22–27, Aug. 1996.
[18] K. E. Graves, P. G. Iovenitti, and D. Toncich, "Electromagnetic regenerative damping in vehicle suspension systems," *J. Veh. Design*, vol. 24, nos. 2 and 3, pp. 182–197, Feb./Mar. 2000.
[19] B. Lequesne, "Permanent magnet linear motors for short strokes," *IEEE Trans. Ind. Applicat.*, vol. 32, no. 1, pp. 161–168, Jan./Feb. 1996.
[20] T. D. Gillespie, "*Fundamentals of Vehicle Dynamics*," Soc. Automobile Eng., 1992.
[21] R. Rajamani and J. K. Hedrick, "Adaptive observers for active automotive suspensions: Theory and experiment," *IEEE Trans. Contr. Syst. Technol.*, vol. 3, no. 1, pp. 86–93, Mar. 1995.
[22] A. Alleyne and J. K. Hedrick, "Nonlinear adaptive control of active suspensions," *IEEE Trans. Contr. Syst. Technol.*, vol. 3, no. 1, pp. 94–101, Jan. 1995.
[23] V. Utkin, J. Guldner, and J. Shi, *Sliding Mode Control in Electromechanical Systems*. London, U.K.: Taylor & Francis, 1999.
[24] J. T. Broch, *Mechanical Vibration and Shock Measurements*. Nærum, Denmark: Brüel & Kjaer, 1984.

Ismenio Martins (M'96) was born in Olhao, Portugal, in 1955. He received the B.Sc. and M.Sc. degrees in electromechanical engineering from the Moscow Power Institute, Moscow, Russia, and the M.Sc. and Ph.D. degrees in electrical engineering from IST—Technical University of Lisbon, Lisbon, Portugal.

He currently holds the positions of Chairman of the Scientific Council and the Director of Department of Electrical Engineering of E.S.T. University of Algarve, Algarve, Portugal.

Dr. Martins is a Member of the Portuguese Engineers Association.

Jorge Esteves (SM'84) received the M.Sc. and Ph.D. degrees in electrical engineering from Instituto Superior Técnico, Lisbon, Portugal, in 1983, 1986, and 1992, respectively.

He was University Professor with Instituto Superior Técnico from 1983 until 2004. In 2004, he joined Instituto Superior de Engenharia de Lisboa as Coordinator Professor at the Department of Electrical and Automation Engineering. He is also researcher from Centro de Automática da Universidade Técnica de Lisboa. His main research interests are electrical machines modelling, variable speed electrical drive and generator systems, and applications of electric and electronic systems to the transports domain.

Dr. Esteves is President of the Board of the Portuguese Electric Vehicle Association. Currently, he is Director of Dispatch and Networks at the Portuguese Energetic Services Regulator (ERSE).

Gil D. Marques (M'95) was born in Benedita, Portugal, on March 24, 1958. He received the Dipl. Ing., and Ph.D. degrees in electrical engineering from the Technical University of Lisbon, Portugal, in 1981 and 1988, respectively.

Since 1981, he has been with the Instituto Superior Técnico, Technical University of Lisbon, where he teaches Power Systems in the Department of Electrical and Computer Engineering. His research interests include electrical machines, static power conversion, variable-speed drive and generator systems, harmonic compensation systems, and distribution systems. He is currently Associate Professor with the Instituto Superior Técnico, Technical University of Lisbon.

Fernando Pina da Silva was born in Lisbon, Portugal, in 1946. He received the M.Sc. degree in mechanical engineering from IST—Technical University of Lisbon in 1971, and the Ph.D. in applied mechanics from the Imperial College of Science and Technology, London, U.K., in 1979.

He currently holds the position of Associate Professor at IST, being responsible for the chairs of Machine Design, Tribology, and Maintenance, and he is also Prof. Coordinator of the Post-Graduate Course in Automotive Technology Maintenance and Management IST.

Dr. da Silva is a Member the Society of Automotive Engineers (USA) and the European Transport Safety Council (Brussels).